

# Enhanced di-Higgs Production through Light Colored Scalars

Graham D. Kribs<sup>1</sup> and Adam Martin<sup>2,3</sup>

<sup>1</sup>*Department of Physics, University of Oregon, Eugene, OR 97403*

<sup>2</sup>*Theoretical Physics Department, Fermilab, Batavia, IL 60510*

<sup>3</sup>*Department of Physics, University of Notre Dame, Notre Dame, IN 46556\**

(Dated: July 20, 2012)

We demonstrate enhanced di-Higgs production at the LHC in the presence of modifications of the effective couplings of Higgs to gluons from new, light, colored scalars. While our results apply to an arbitrary set of colored scalars, we illustrate the effects with a real color octet scalar – a simple, experimentally viable model involving a light ( $\simeq 125$ – $300$  GeV) colored scalar. Given the recent LHC results, we consider two distinct scenarios: First, if the Higgs is indeed near 125 GeV, we show that the di-Higgs cross section could be up to nearly  $10^3$  times the Standard Model rate for particular octet couplings and masses. This is potentially observable in *single* Higgs production modes, such as  $pp \rightarrow hh \rightarrow \gamma\gamma b\bar{b}$  as well as  $pp \rightarrow hh \rightarrow \tau^+\tau^- b\bar{b}$  where a small fraction of the  $\gamma\gamma$  or  $\tau^+\tau^-$  events near the putative Higgs invariant mass peak contain also a  $b\bar{b}$  resonance consistent with the Higgs mass. Second, if the Higgs is not at 125 GeV (and what the LHC has observed is an impostor), we show that the same parameter region where singly-produced Higgs production can be suppressed below current LHC limits, for a heavier Higgs mass, also simultaneously predicts substantially enhanced di-Higgs production. We point out several characteristic signals of di-Higgs production with a heavier Higgs boson, such as  $pp \rightarrow hh \rightarrow W^+W^-W^+W^-$ , which could use same-sign dileptons or trileptons plus missing energy to uncover evidence.

## I. INTRODUCTION

Di-Higgs production in the Standard Model (SM) has a very small rate at the LHC [1–4]. For  $m_h = 125$  GeV, the leading order cross section is  $\sigma(pp \rightarrow hh) = 4$  (16) fb at  $\sqrt{s} = 8$  (14) TeV. This is much smaller than the single Higgs production cross section due to the larger partonic energy needed to produce two Higgs bosons, as well as an accidental cancellation between the  $s$ -channel and box diagram contributions to the amplitude  $gg \rightarrow hh$ . Hence, like other accidentally suppressed processes in the Standard Model, di-Higgs production provides a great opportunity for new physics to be observed. In this paper we demonstrate that in the presence of a general set of light colored scalars, the di-Higgs production cross section can be enhanced by orders of magnitude above the Standard Model rate. Light colored scalars that couple to the Higgs boson are well known to have a profound effect on *single* Higgs production [5–13]. Di-Higgs production has been considered previously in several different contexts [14–36].

Since direct searches at the LHC for light colored scalars that couple to the Higgs have many constraints, depending on the model and the decay modes, the burden is on us to provide a “benchmark model” that evades these constraints while providing the enhancements in di-Higgs production that we find. Several possible representations could be considered, including the superpartners to the top, vector-like sets of particles (that may or may

not carry electroweak quantum numbers), or real representations such as an electroweak neutral color octet.

A real scalar octet is an interesting example of a colored scalar that can be effectively hidden in the LHC data. In the model that we consider, these scalars are pair-produced (up to small corrections coming from loop processes), and decay through loop-level processes to a pair of gluons. Thus, the signature is two pairs of jets with equal invariant mass, making four total jets. ATLAS [37] and CMS [38] have multi-jet searches that are potentially sensitive to this scalar; the ATLAS study restricts  $M_S \gtrsim 125$  GeV, while the CMS study [38] is sensitive only for scalars exceeding 320 GeV. This leaves a wide range of real scalar color octets allowed by LHC constraints. A real scalar color octet  $S_a$  can couple to the Higgs boson through the renormalizable Higgs-portal interaction of the form  $(\kappa/2)S_a^2 H^\dagger H$ . Vital to our study is the possibility that  $\kappa$  can be negative, as we will see.

The correlation between effects in single-Higgs and di-Higgs production has been studied previously in terms of contact interactions [26, 29]. For very heavy colored scalars – meaning scalars whose mass is large compared to the electroweak scale,  $M_i \gg v$ , as well as to the characteristic energy of di-Higgs production (roughly  $M_i \gg \hat{s} \sim \mathcal{O}(10 m_h^2)$ ) – the effective operators provide a reasonable description. As we will see, for the colored scalars we consider in this paper, between about 100 to 300 GeV, the full momentum-dependence of the one-loop calculation is essential to accurately estimate the di-Higgs enhancement. We show this explicitly in Appendix B.

Finally, it may seem somewhat quixotic that we consider  $m_h = 125$  GeV as well as  $m_h > 125$  GeV, given the

\* visiting scholar

strong evidence from the LHC for a new particle with properties consistent with a Higgs near  $m_h = 125$  GeV [39, 40]. While much work remains to be done to verify that the 125 GeV particle is indeed the (or a) Higgs boson, there is a more direct reason for our continued interest in a heavier Higgs boson. As we showed in Ref. [12], colored scalars can *suppress* single Higgs production well below the current bounds from LHC for a wide range of Higgs masses. So the argument that “we have already searched for a heavier Higgs boson and did not find it, so the Higgs must be the 125 GeV Higgs-like particle” is simply wrong. This reasoning is wrong because the argument applies *only* to the Standard Model. The general class of models we consider in this paper – colored scalars with Higgs portal couplings – provide a clear class of counterexamples. Of course we are not disputing the strong evidence for a 125 GeV particle; instead, we believe maintaining a healthy dose of skepticism regarding the true identity of this particle, given the wide number of impostors [41] that could be masquerading as a Higgs-like resonance.

## II. EFFECTIVE COUPLINGS

Low energy theorems for Higgs physics provide powerful methods to determine the effective Higgs couplings to both Standard Model particles as well as new physics [15, 42–46]. We are interested in extending the Standard Model to include a general set of colored scalars  $\phi_i$  in arbitrary representations of QCD. The multiplicity of scalars (number of flavors) is taken into account, while our predictions for the single and di-Higgs rates are otherwise independent of the electroweak quantum numbers at leading order in the couplings.

The minimal Lagrangian for colored scalars in complex representations is

$$\mathcal{L}_c = (D_\mu \phi_i)^\dagger (D^\mu \phi_i) - m_i^2 \phi_i^\dagger \phi_i - \kappa_i \phi_i^\dagger \phi_i H^\dagger H \quad (1)$$

while for real scalars the Lagrangian is

$$\mathcal{L}_r = \frac{1}{2} (D_\mu \phi_i)^2 - \frac{1}{2} m_i^2 \phi_i^2 - \frac{\kappa_i}{2} \phi_i^2 H^\dagger H. \quad (2)$$

We have not included quartic (or possibly cubic) self-interactions, nor interactions among different *flavors* of scalars, since these couplings will not play any role in our calculations of di-Higgs production. The field-independent scalar mass-squared is

$$M_i^2 \equiv m_i^2 + \frac{\kappa_i v^2}{2}, \quad (3)$$

while the Higgs field-dependent mass is

$$M_i^2(h) = m_i^2 + \frac{\kappa_i}{2} (v + h)^2, \quad (4)$$

both of which apply to scalars in real or complex representations. When  $m_h \ll M_i$ , the colored scalars can be integrated out, resulting in an effective theory in powers

of  $1/M_i$ . The leading interactions of the Higgs to gluons can be determined by matching the strong coupling constant in the low energy and high energy theory [45],

$$\begin{aligned} \mathcal{L}_{\text{eff}} &= -\frac{1}{4} \frac{1}{g_{\text{eff}}^2(\mu, h)} G_{\mu\nu}^a G^{a\mu\nu} \\ &= -\frac{1}{4} \left[ \frac{1}{g^2(\mu)} - \frac{1}{12\pi^2} \log \frac{m_t(h)}{\mu} \right. \\ &\quad \left. - \sum_i \frac{C_i}{24\pi^2} \log \frac{M_i(h)}{\mu} \right] G_{\mu\nu}^a G^{a\mu\nu} \end{aligned} \quad (5)$$

where we have included the top quark and an arbitrary set of colored scalars with explicit Higgs field-dependence. For a real scalar field,  $C_i$  is the Dynkin index, e.g.  $C_i = 3$  for a color octet; for a complex representation, replace  $C_i \rightarrow 2C_i$ . This leads to the one-loop effective Lagrangian,

$$\frac{\alpha_s}{12\pi} \left[ \log m_t(h) + \sum_i \frac{C_i}{2} \log M_i(h) \right] G_{\mu\nu}^a G^{a\mu\nu}, \quad (6)$$

where we have shifted  $G_{\mu\nu}^a$  back to the canonical basis.

Expanding Eq. (6) to first order in  $h/v$ , we obtain the single Higgs effective interaction with colored scalars,

$$\frac{h}{v} G_{\mu\nu}^a G^{a\mu\nu} \sum_i \frac{\alpha_s}{48\pi} C_i \frac{\kappa_i v^2}{M_i^2}. \quad (7)$$

The single Higgs effective interaction, Eq. (7), is for example identical to the result obtained from our previous study of Higgs suppression through colored scalars in the limit  $m_h \ll M_i$  [Eq. (2.7) from Ref. [12]].

The 4-point di-Higgs effective interaction is similarly obtained,

$$\frac{h^2}{2v^2} G_{\mu\nu}^a G^{a\mu\nu} \sum_i \frac{\alpha_s}{48\pi} C_i \left( \frac{\kappa_i v^2}{M_i^2} - \frac{\kappa_i^2 v^4}{M_i^4} \right). \quad (8)$$

The top quark contributions to the effective couplings can also be obtained by expanding Eq. (6),

$$\frac{\alpha_s}{12\pi} \left( \frac{h}{v} - \frac{h^2}{2v^2} \right) G_{\mu\nu}^a G^{a\mu\nu}. \quad (9)$$

There are two critical observations we can make at the effective interaction level. First, when  $M_i > \sqrt{|\kappa_i|}v$ , the relative *sign* of the the top quark contribution to the effective operator  $h^2 G_{\mu\nu}^a G^{a\mu\nu}$  is opposite (the same as) that of the scalar contribution when  $\kappa_i > 0$  ( $\kappa_i < 0$ ). Second, in the limit  $m_h, v \ll M_i$ , we see that the same coefficient that determines the single Higgs effective interaction also uniquely determines the di-Higgs effective interaction. This will be important for gaining some qualitative understanding of our di-Higgs cross section results.

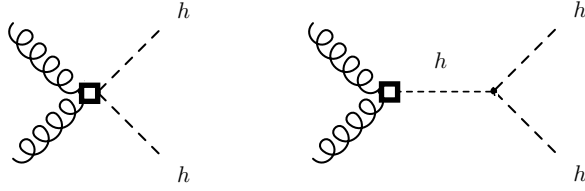


FIG. 1. Effective operator contributions to  $gg \rightarrow hh$ .

### III. CONTRIBUTIONS TO DI-HIGGS PRODUCTION

We now carry out the calculation of di-Higgs production at a hadron collider. Light quarks play no role in the leading-order di-Higgs production cross section, so we are left with the gluon-induced partonic process  $gg \rightarrow hh$ . We calculate the amplitudes for di-Higgs production in two independent methods. First we calculate the amplitudes using the effective interactions derived in Sec. II. This allows us to obtain simple, analytic formulae that provide several qualitative features of the full calculation. Next, we carry out a full momentum-dependent one-loop calculation of  $gg \rightarrow hh$  including top quarks and an arbitrary set of colored scalars.

The amplitude for  $gg \rightarrow hh$  can be decomposed into two non-interfering Lorentz structures following Ref. [1],

$$\mathcal{M}(g_a g_b \rightarrow hh)_{\mu\nu} = \mathcal{P} P_{\mu\nu} \delta_{ab} + \mathcal{Q} Q_{\mu\nu} \delta_{ab}, \quad (10)$$

where

$$P_{\mu\nu} = \eta_{\mu\nu} - \frac{p_{1\nu} p_{2\mu}}{(p_1 \cdot p_2)} \quad (11)$$

$$Q_{\mu\nu} = \eta_{\mu\nu} + \frac{m_H^2 p_{1\nu} p_{2\mu}}{p_T^2 p_1 \cdot p_2} - \frac{2(p_1 \cdot k_1) p_{2\mu} k_{1\nu}}{p_T^2 p_1 \cdot p_2} - \frac{2(p_2 \cdot k_1) p_{1\nu} k_{1\mu}}{p_T^2 p_1 \cdot p_2} + \frac{2k_{1\mu} k_{1\nu}}{p_T^2}. \quad (12)$$

In these formula,  $p_1$  and  $p_2$  are the incoming momenta of the gluons,  $k_1$  is the outgoing momenta of one of the Higgs bosons, and  $p_T$  is the transverse momenta of the Higgs:  $p_T^2 = (\hat{u} \hat{t} - m_H^4)/\hat{s}$ . The  $Q_{\mu\nu}$  is the only possible alternative Lorentz structure once the Ward identities and orthogonality to  $P_{\mu\nu}$  have been imposed.

#### A. Di-Higgs Amplitude from Effective Couplings

The effective couplings given by Eqs. (7), (8), and (9) lead only to contributions to the  $P_{\mu\nu}$  structure. The Feynman diagrams include both the 4-point effective interaction  $h^2 G_{\mu\nu}^a G^{a,\mu\nu}$  as well as the diagram with  $s$ -channel Higgs exchange involving the 3-point effective interaction  $h G_{\mu\nu}^a G^{a,\mu\nu}$  and the triple-Higgs self-interaction, shown in Fig. 1. We obtain

$$\mathcal{P}_{\text{top}}^{\text{eff}} = \frac{\alpha_s}{3\pi v^2} \left( -1 + \frac{3m_h^2}{\hat{s} - m_h^2} \right) \quad (13)$$

$$\mathcal{P}_{\text{scalar}}^{\text{eff}} = \sum_i \frac{\alpha_s \kappa_i C_i}{24\pi M_i^2} \left( 1 + \frac{3m_h^2}{\hat{s} - m_h^2} - \frac{\kappa_i v^2}{M_i^2} \right), \quad (14)$$

where we have neglected the width of Higgs in the  $s$ -channel propagators. The top quark contributions to the amplitude interfere destructively. This, combined with the necessity to sample parton distribution functions at larger  $x$  (to obtain larger  $\hat{s}$ ), is the central reason that the di-Higgs production cross section at a hadron collider is so small in the Standard Model.

The amplitudes derived from the effective interactions allow us to make several interesting qualitative observations about the scalar contributions:

- For  $\kappa_i > 0$  with  $M_i \gtrsim \sqrt{|\kappa_i|}v$ , the top contribution and the scalar contributions destructively interfere, weakening the effects of colored scalars on di-Higgs production.
- For  $\kappa_i < 0$  with  $M_i \gtrsim \sqrt{|\kappa_i|}v$ , the top contribution and the scalar contributions constructively interfere, strengthening the effects of colored scalars on di-Higgs production.
- When  $M_i \lesssim \sqrt{|\kappa_i|}v$ , the third contribution in Eq. (14) begins to affect the scalar amplitude for di-Higgs production. However, momentum-dependent corrections proportional to  $\hat{s}/M_i^2$  are at least as important, since  $\hat{s} \geq 4m_h^2$ . In this region, the  $1/M_i$  expansion is no longer valid, and we need the full momentum-dependent loop functions to make accurate quantitative calculations.

The two main results we find from the di-Higgs amplitudes calculated with the effective operators are that: i.) we expect a considerably larger cross section when  $\kappa_i < 0$ , and  $M_i \gtrsim \sqrt{|\kappa_i|}v$ ; ii.) we expect a strong correlation between single Higgs production and di-Higgs production once  $M_i$  is large enough for the effective operators to reproduce the full momentum-dependent one-loop results.

#### B. Di-Higgs Amplitude at One-Loop

We now turn to the full one-loop leading-order calculation of di-Higgs production including the top quark and the scalars. The Standard Model contribution to  $gg \rightarrow hh$  comes from top quark triangle diagrams stitched to a triple-Higgs vertex via a Higgs boson propagator, as well as box diagrams with two top Yukawa coupling insertions. The full momentum-dependent expressions for  $\mathcal{P}$ ,  $\mathcal{Q}$  for the top contributions can be found in Ref. [1].

The scalar octet loops can be similarly classified into triangles and boxes (or by powers of the Higgs-portal coupling  $\kappa$ ). The complete set of (leading order) diagrams are shown below in Fig. 2. The scalar triangle diagram

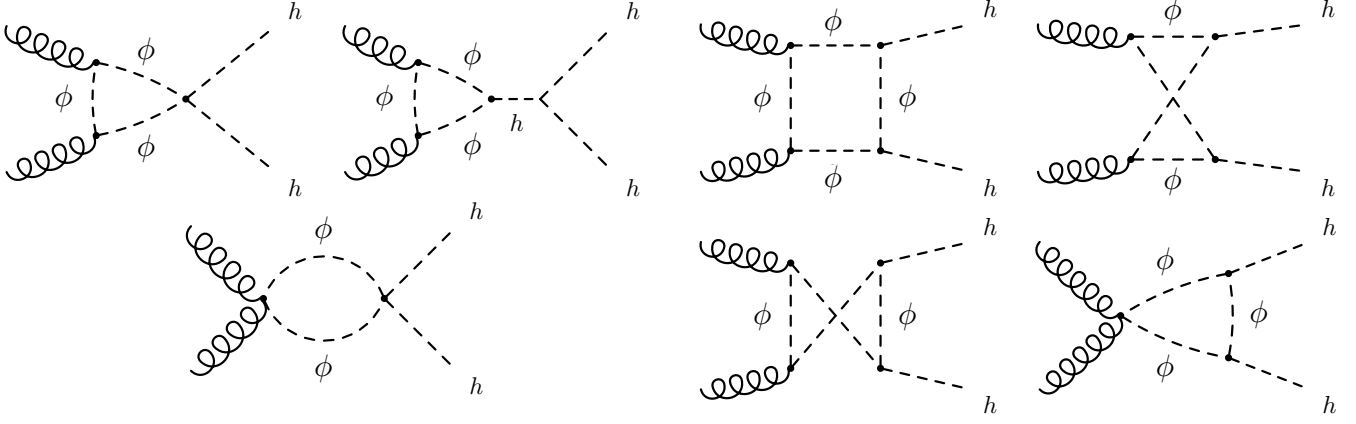


FIG. 2. Scalar loop contributions to  $gg \rightarrow hh$ . The three diagrams on left are  $\mathcal{O}(\alpha_s \kappa)$ , while the four diagrams on the right are  $\mathcal{O}(\alpha_s \kappa^2)$ , where  $\kappa$  is the Higgs-portal coupling.

contributions only have  $P_{\mu\nu}$  gauge structure:

$$\mathcal{P}_{\text{tri}} = \sum_i \frac{\alpha_s \kappa_i C_i}{4\pi} \left( 1 + \frac{3m_h^2}{\hat{s} - m_h^2} \right) \times (2M_i^2 C_0(p_1, p_2 : M_i) + 1). \quad (15)$$

The first term in the parenthesis comes from attaching the 4-point vertex in the  $\kappa$  interaction to the scalar loop,

while the second term comes from connecting a Higgs propagator and 3-point vertex to the triple-Higgs self-interaction.

The box diagrams involving scalars (as well as top quarks) contribute to both  $(P_{\mu\nu}, Q_{\mu\nu})$  Lorentz structures. We evaluate the scalar contribution to  $\mathcal{P}$  and  $\mathcal{Q}$  (as well as  $\mathcal{P}_{\text{tri}}$  in Eq. (15)) in terms of the Passarino-Veltman one-loop functions given in Appendix A. We obtain:

$$\mathcal{P}_{\text{box}} = \sum_i \frac{\alpha_s v^2 \kappa_i^2 C_i}{2\pi} \times \left[ \frac{m_h^2 - \hat{t}}{\hat{s}} C_0(p_1, k_1 : M_i) + \frac{m_h^2 - \hat{u}}{\hat{s}} C_0(p_2, k_1 : M_i) + M_i^2 (D_0(p_1, p_2, k_1 : M_i) + D_0(p_2, p_1, k_1 : M_i)) + \frac{\hat{u} \hat{t} + 2M_i^2 \hat{s} - m_h^4}{2\hat{s}} D_0(k_1, p_1, p_2 : M_i) \right], \quad (16)$$

$$\mathcal{Q}_{\text{box}} = \sum_i \frac{\alpha_s v^2 \kappa_i^2 C_i}{2\pi} \times \frac{1}{2(m_h^4 - \hat{t} \hat{u})} \left[ \hat{s} (\hat{u} + \hat{t}) C_0(p_1, p_2 : M_i) - (\hat{u}^2 + \hat{t}^2 - 2m_h^4) C_0(k_1, k_2 : M_i) + 2\hat{t} (\hat{t} - m_h^2) C_0(p_1, k_1 : M_i) + 2\hat{u} (\hat{u} - m_h^2) C_0(p_2, k_1 : M_i) + 2M_i^2 (m_h^4 - \hat{t} \hat{u}) D_0(k_1, p_1, p_2 : M_i) + (2M_i^2 (m_h^4 - \hat{t} \hat{u}) - \hat{s} \hat{t}^2) D_0(p_1, p_2, k_1 : M_i) + (2M_i^2 (m_h^4 - \hat{t} \hat{u}) - \hat{s} \hat{u}^2) D_0(p_2, p_1, k_1 : M_i) \right]. \quad (17)$$

Adding the scalar loop  $\mathcal{P}, \mathcal{Q}$  to the top loop contributions gives us the total  $\mathcal{M}(gg \rightarrow hh)_{\mu\nu}$  amplitude. Squaring and adding phase space, color- and spin-averaging factors, we arrive at the differential partonic cross section,

$$\frac{d\hat{\sigma}(gg \rightarrow hh)}{d \cos \theta^*} = \frac{\beta_h}{1024 \pi \hat{s}} (|\mathcal{P}_{\text{tot}}|^2 + |\mathcal{Q}_{\text{tot}}|^2). \quad (18)$$

Note that the overall factor of 1/2 for creating a pair of identical particles is canceled by  $P_{\mu\nu} P^{\mu\nu} = Q_{\mu\nu} Q^{\mu\nu} = 2$ .

#### IV. BENCHMARK COLOR OCTET MODEL

We now specialize our results to our benchmark model: a single real, color-octet, electroweak neutral scalar  $S_a$  [12, 47–49],

$$\mathcal{L}_S = \frac{1}{2} (D_\mu S_a)^2 - \frac{1}{2} M_S^2 (S_a)^2 - \frac{\kappa}{2} (S_a)^2 H^\dagger H - \frac{\omega}{4} (S_a)^4 - \mu_S d^{abc} S_a S_b S_c. \quad (19)$$

Here we have included one Higgs-portal interaction, with coupling  $\kappa$ , as well as additional renormalizable self-interactions among the  $S_a$ : a quartic interaction with

coupling  $\omega$ , and a cubic interaction with (dimensionful) coupling  $\mu_S$ . The cubic interaction implies the  $S_a$  can decay into two gluons through a triangle loop. Since the Lagrangian possesses a  $\mathbb{Z}_2$  symmetry when  $\mu_s = 0$ , small values of  $\mu_S$  are technically natural. This allows us to assume that  $\mu_S$  is large enough to cause prompt  $S_a$  decays, but is otherwise small enough to not play a role in our calculations of di-Higgs production.

The effect on single Higgs production of light scalars through the Higgs-portal interaction was precisely the subject of our Ref. [12]. There we showed that single Higgs production could be dramatically reduced for a wide range of *negative*  $\kappa$ , and scalar masses in the range  $M_S \sim 100\text{--}300$  GeV. The reduction comes from destructive interference between the top quark loop and the loop of  $S_a$ . The suppression could reach 75 – 90% without excessive tuning. For the most extreme cancellation, relatively large couplings  $\kappa \sim -1$  and light scalars  $M_S \lesssim 200$  GeV were required. Taking even lighter scalar masses, the scalar loop contributions can overwhelm the top quark contribution, and the single Higgs production cross section can again be  $\mathcal{O}(1)$  times the Standard Model value.

As was discussed in Ref. [12], color octet scalars are dominantly pair-produced and decay (via a loop of  $S_a$ ) to a pair of gluons. Thus, the signature is two pairs of jets with equal invariant mass, making four total jets. This signature provides a handle to help distinguish it from the multi-jet background. However, when the scalars are light, they create relatively soft jets that are not efficiently triggered on due to the large background. In addition to the large rate and combinatorial hurdles, extracting the signal is further complicated by pileup. A comparison between ATLAS [37] and CMS [38] multi-jet searches demonstrates the difficulties in placing constraints in higher luminosity runs. The ATLAS [37] search was able to disfavor real color octet scalar between 100–125 GeV. The low reach in  $M_S$  was possible because this study was performed with  $36\text{ pb}^{-1}$  of data where the luminosity was sufficiently low that trigger thresholds could be kept small. The CMS [38] search, by contrast, was performed on  $1\text{ fb}^{-1}$  of data, where the jet trigger threshold was 70 GeV. This prevented the CMS study to be sensitive to objects lighter than 300 GeV.<sup>1</sup> By adopting specialized pre-scaled triggers at lower jet  $p_T$ , improvements to the low mass octet search may be possible, but to the best of our knowledge, no such studies have been completed.

It is also important to consider the possible range of the dimensionless Higgs-portal coupling  $\kappa$ , particularly for negative values. Large negative  $\kappa$  could destabilize the scalar potential at large field values. The naive tree-level bound can be obtained by rewriting the quartic interactions of the scalar potential as  $(\sqrt{\omega}(S_a)^2 - \sqrt{\lambda_h}H^\dagger H)^2 +$

$2\sqrt{\omega\lambda_h}S_a^2H^\dagger H$ , and thus  $|\kappa| < 2\sqrt{\omega\lambda_h}$  [10] where  $\lambda_h$  is the Higgs quartic coupling. However, in Appendix C we calculate the renormalization group equations for  $\kappa$ ,  $\omega$ , and  $\lambda_h$ , showing that negative  $\kappa$  runs rapidly to smaller (absolute) values at a larger renormalization scale. This suggests that the bounds on negative  $\kappa$  are expected to be significantly relaxed once one uses the renormalization-group improved potential.

## V. ENHANCED DI-HIGGS PRODUCTION

We now calculate the di-Higgs production cross section for two distinct scenarios:  $m_h = 125$  GeV, and  $m_h > 125$  GeV. In the case  $m_h = 125$  GeV, we consider both negative and positive  $\kappa$ , since a wide range of  $(\kappa, M_S)$  parameter space is allowed by a (generous) interpretation of the 125 GeV resonance observed by LHC as a Higgs boson. For  $m_h > 125$  GeV, we consider only negative  $\kappa$ , since this is the only region of  $(\kappa, M_S)$  space where the (heavy) single Higgs production can be suppressed below the LHC bounds [12].

### A. $m_h = 125$ GeV

We are finally in a position to evaluate the di-Higgs production cross section, Eq. (18), comparing to the Standard Model value while scanning over the scalar parameters  $M_S$  and  $\kappa$ . In Fig. 3 we show numerical results for the ratio  $\sigma(pp \rightarrow hh)_{\text{top+scalar}}/\sigma(pp \rightarrow hh)_{\text{top}}$  as a function of  $M_S$  and  $\kappa$  for LHC at  $\sqrt{s} = 8$  TeV. The scalar and top calculations were performed at leading order; however by taking a ratio to the Standard Model result, higher order corrections in  $\alpha_s$  to di-Higgs production should largely cancel out. Fig. 3 contains three plots: one with positive and negative  $\kappa$  with  $M_S < 400$  GeV; and two “zoomed in” plots that more easily demonstrate the large effects at smaller  $M_S$  for both positive and negative  $\kappa$ . These contours are overlaid onto colored regions that show the single Higgs production ratio  $\sigma(pp \rightarrow h)_{\text{top+scalar}}/\sigma(pp \rightarrow h)_{\text{top}}$ , derived from Ref. [12]. We see that once  $M_S \gtrsim m_h$ , the di-Higgs production contours follow the single Higgs production region shapes fairly well. This was partly anticipated from the coefficients of the effective operators, Eqs. (7),(8), that were found to be the same for  $h/vG_{\mu\nu}^a G^{a,\mu\nu}$  and  $h^2/(2v^2)G_{\mu\nu}^a G^{a,\mu\nu}$ . Interestingly, the *magnitude* of the di-Higgs production cross section is not estimated particularly well from the effective operators. In Appendix B we compare the results for the exact momentum-dependent one-loop calculation and the effective effective operators. This we do by showing the negative  $\kappa$  “zoomed in” plot identical to Fig. 3(c) overlaid with the effective operator results. It is perhaps not surprising that these results do not agree, since the effective operators neglect momentum-dependent corrections of order  $\hat{s}/M_i^2$  that is order one or larger in the region we show. Perhaps more interesting, however, is that

<sup>1</sup> The jet  $p_T$  cut was 150 GeV in this study.

the effective operators do reproduce the *shape* of the contours of the di-Higgs cross section ratio in  $(\kappa, M_S)$  when the ratio  $\sigma(pp \rightarrow hh)_{\text{scalar+top}}/\sigma(pp \rightarrow hh)_{\text{top}}$  itself is large (say,  $\gtrsim 10$ ) and  $M_S \gtrsim m_h$ . Of course in the region  $M_S < m_h$ , as well as when the ratio itself is relatively small (say,  $\lesssim 10$ ), the effective operators do not reproduce either the magnitude or shape of the cross section ratio results.

If we generously allow the recent LHC results to suggest  $0.5 < \sigma(pp \rightarrow h)_{\text{scalar+top}}/\sigma(pp \rightarrow h)_{\text{top}} < 2$ , then there are three regions of interest:

- Negative  $\kappa$ , below and to the left of the red region. This region has the largest di-Higgs cross section enhancement, since it is the region with largest negative  $\kappa$  for a given  $M_S$ . In this region the scalar contributions to the single Higgs production are roughly twice the size, but opposite in sign, to the top contribution, resulting in a single Higgs production rate that can be smaller, the same as, or larger than the SM single Higgs production rate. The di-Higgs cross section, by contrast, is *enormous* – between several roughly 100-1000 times the Standard Model cross section.
- Negative  $\kappa$ , above and to the right of the red region. This region has a single Higgs production cross section that is smaller than the Standard Model. Nevertheless, the di-Higgs production cross section can be up to about 10 times the Standard Model rate. In this region there is a strong correlation between (slight) suppression of the single Higgs production rate and the (much larger) enhancement of the di-Higgs production rate.
- Positive  $\kappa$ . In this region, the single Higgs production rate is larger than the Standard Model. Restricting to  $\sigma(pp \rightarrow h)_{\text{scalar+top}}/\sigma(pp \rightarrow h)_{\text{top}} < 2$ , we see the di-Higgs enhancement is negligible. It is in this region that smaller positive  $\kappa$  leads to constructive interference for single Higgs production and destructive interference for di-Higgs production.

### B. $m_h > 125$ GeV

Consider now the case where the 125 GeV particle observed by LHC is, in fact, an imposter. As we showed in Ref. [12], there is viable parameter region where the Higgs can be much heavier, and yet, be safe against the LHC search bounds on single Higgs production. This occurs when the colored scalar contributions to single Higgs production interfere destructively with the top contribution, leading to a large region of highly suppressed single Higgs production rate at LHC. We show this in Fig. 4, where the viable region lies entirely in the red and some of the blue region, where the single Higgs cross section at LHC,  $\sigma(pp \rightarrow h)_{\text{scalar+top}}/\sigma(pp \rightarrow h)_{\text{top}} < 0.1\text{-}0.25$ .

Here we see that there is a perfect correlation between *suppression* of single Higgs production and *enhancement* of di-Higgs production. This occurs for all of the Higgs masses shown, with the largest di-Higgs enhancement occurring for the smaller Higgs masses,  $m_h = 160, 200$  GeV, large negative  $\kappa$ , and  $M_S \lesssim 250$  GeV. Here the enhancement is between about 5 to 200 times the Standard Model rate (for the given Higgs mass). This is the smoking gun for a heavy hidden Higgs boson in the case where the 125 GeV particle is an imposter.

### C. Kinematic Distributions of Enhanced Di-Higgs Production

In addition the large increase in the di-Higgs production rate, there are also modifications to the kinematical distributions of di-Higgs production. Here we turn to Monte Carlo to simulate the signal. We implemented the  $gg \rightarrow hh$  processes into **MadGraph4** [50] by modifying the necessary **HELAS** [51, 52] routines, including both Lorentz structures ( $P_{\mu\nu}$  and  $Q_{\mu\nu}$ ) and retained the full momentum dependence. To evaluate the Passarino-Veltman one-loop functions, the  $gg \rightarrow h, gg \rightarrow hh$  amplitudes were interfaced with the **LoopTools** [53] package. We utilize CTEQ6L1 parton distribution functions with the scale choice  $\mu_F = \mu_R = 2 \times m_h$  for all simulations.

We first look to basic kinematic distributions of the Higgs bosons. The  $p_T$  and rapidity ( $Y_h$ ) spectra are shown below in Fig. 5 for several choices of  $M_S$ ; the distributions are area-normalized to focus on the shape difference. Note that the  $p_{T,h}$  spectrum peaks roughly at the mass of the particle dominating the loops, near  $m_t$  in the SM and  $M_S$  in all non-SM cases. For the SM case this feature can be traced to an enhancement in the diagrams when  $\hat{s} \sim m_t^2$  [1]. A similar enhancement occurs in the scalar loops at  $\hat{s} \sim M_S^2$ . However, unlike in the SM where the triangle and box diagrams always destructively interfere, the interference among the various scalar diagrams depends on the sign of  $\kappa$ , as we have seen. For positive  $\kappa$ , the scalar boxes and triangles also interfere destructively. The severity of the interference depends on  $|\kappa|$ , since the box contributions grow as  $\mathcal{O}(\kappa^2)$ , whereas the triangles,  $\mathcal{O}(\kappa)$ .

In Fig. 5 the Higgs-portal coupling was fixed to  $\kappa = -1$ , while the scalar mass was varied. However, as there are both  $\mathcal{O}(\kappa)$  and  $\mathcal{O}(\kappa^2)$  contributions to  $gg \rightarrow hh$  (at amplitude level), each weighted by different kinematic functions, the  $p_{T,h}$  spectrum does carry some  $\kappa$  dependence. As we can see from Fig. 6, which shows the overlaid  $p_{T,h}$  spectra for three different  $\kappa$  values and fixed  $M_S = 150$  GeV, the  $\kappa$  dependence is fairly small.

Next, we come to the differences between using effective operators and retaining the full one-loop momentum-dependence. In Fig. 7, we take  $M_S = 150$  GeV,  $\kappa = -1$  and compare the  $p_{T,h}$  distributions between using the effective operators [Eqs. (13)-(14)] against the one-loop results [Eqs. (15)-(17)]. Clearly, the distributions are qual-

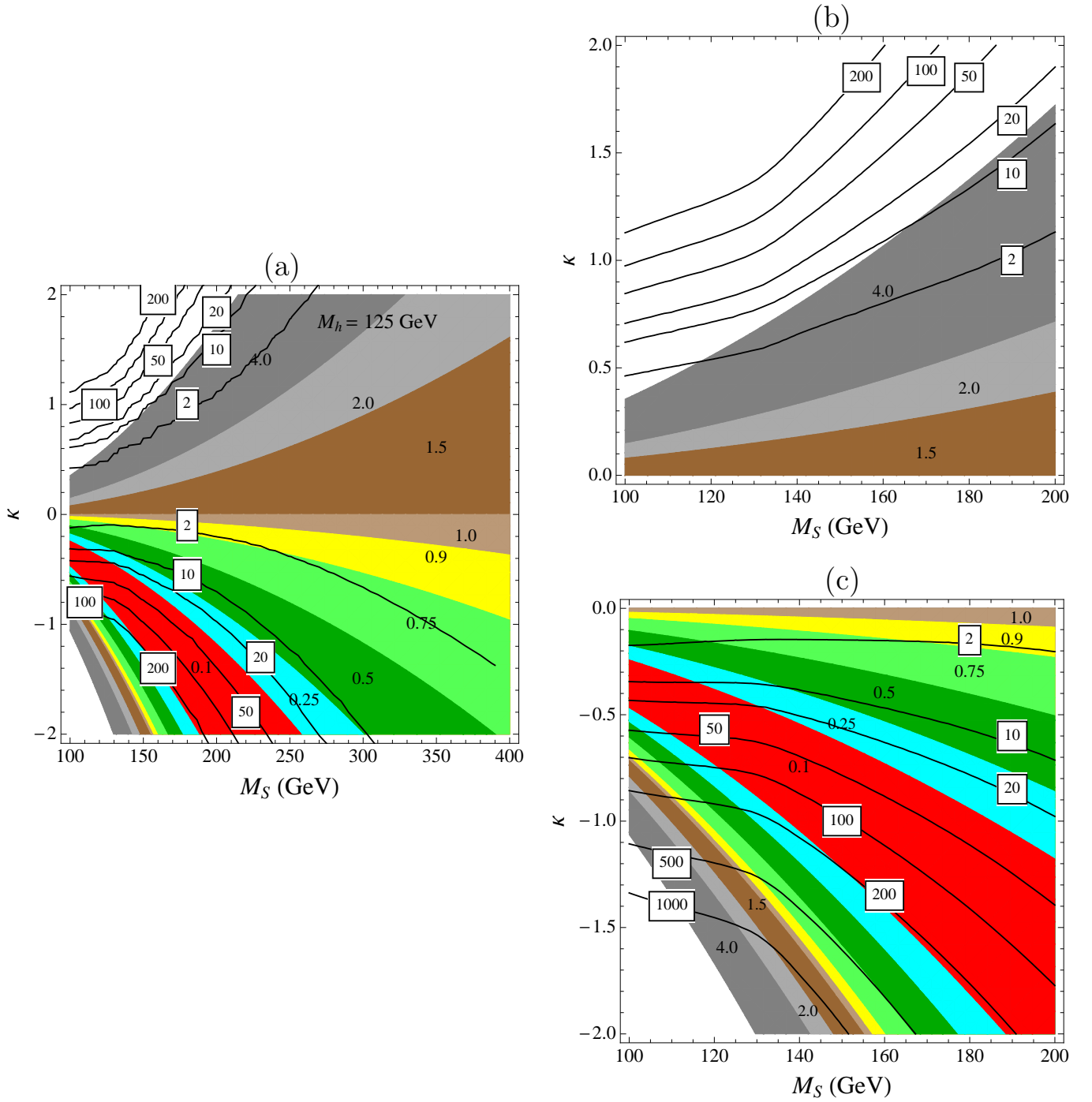


FIG. 3. Di-Higgs as well as single Higgs production cross sections normalized to the Standard Model values. The solid lines show  $\sigma(pp \rightarrow hh)_{\text{scalar+top}}/\sigma(pp \rightarrow hh)_{\text{top}}$ , while the colored regions show when  $\sigma(pp \rightarrow h)_{\text{scalar+top}}/\sigma(pp \rightarrow h)_{\text{top}}$  is less than the numerical value labeling each region. Panels (b) and (c) are “zoomed in” versions of panel (a), to more clearly see the contours in the light  $M_S < 200$  GeV region.

itatively distinct throughout the  $p_{T,h}$  range. For the effective operator calculation, the high- $p_T$  tail is governed by kinematics alone, where as there is an extra suppression from the form factors once we incorporate momentum dependence. An accurate  $p_T$  spectra is vital for phenomenology; the Higgs  $p_T$  will be transferred to its

decay remnants, and the details of the remnant kinematics are a necessary ingredient for successfully separating signal from SM background, regardless of the identity of the final state particles.

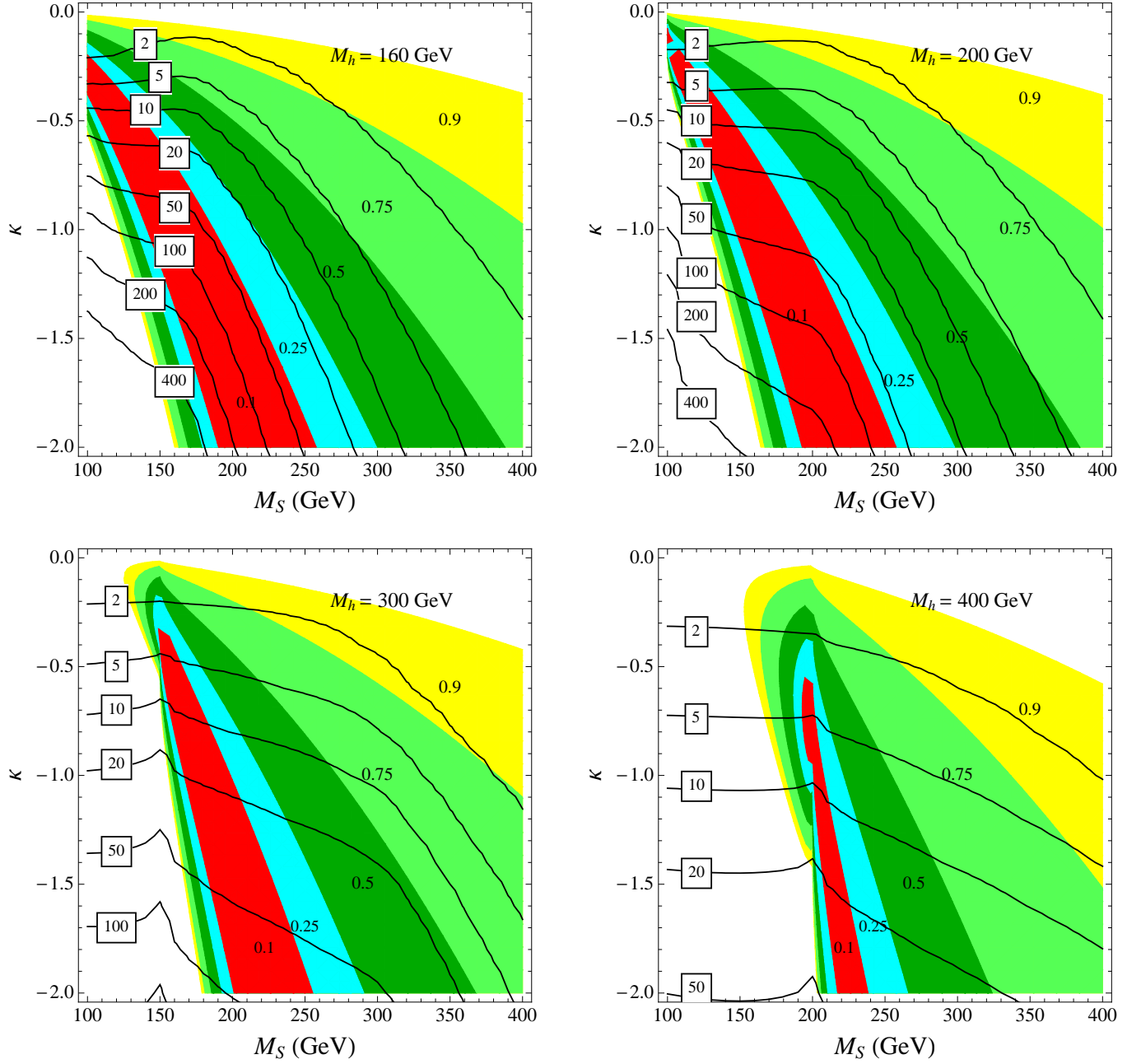


FIG. 4. Same as Fig. 3, but for heavier Higgs masses (assuming the 125 GeV particle observed by LHC is an imposter). The viable parameter space is roughly in the red and blue regions where  $\sigma(pp \rightarrow h)_{\text{scalar+top}}/\sigma(pp \rightarrow h)_{\text{top}} \lesssim 0.25$ . Whenever  $m_h > 2M_S, 2m_t$  there is little space for a suppressed  $\sigma(pp \rightarrow h)$ . This occurs because the loop contributions to the amplitude become complex, and cancellation must be arranged simultaneously between the real and imaginary parts of the top quark and scalar loops.

## VI. DISCOVERING DI-HIGGS

The signals and discovery strategies for di-Higgs production crucially depend on the mass of the Higgs boson and how much the rate is enhanced. We will not attempt to cover all scenarios, and instead focus on two distinct cases:  $m_h = 125$  GeV and  $m_h = 200$  GeV. The  $m_h = 200$  GeV scenario is fairly representative of

a generic heavier Higgs mass ( $m_h \gtrsim 200$  GeV), since the branching fractions into massive gauge bosons dominate. We will sketch the best signals for each case and consider strategies to improve the discovery potential. A detailed study of the full background rates and the optimal cut strategy for a given Higgs mass is beyond the scope of this work.

In the case  $m_h = 125$  GeV (where the particle observed by LHC is taken to be the Higgs boson), the rate



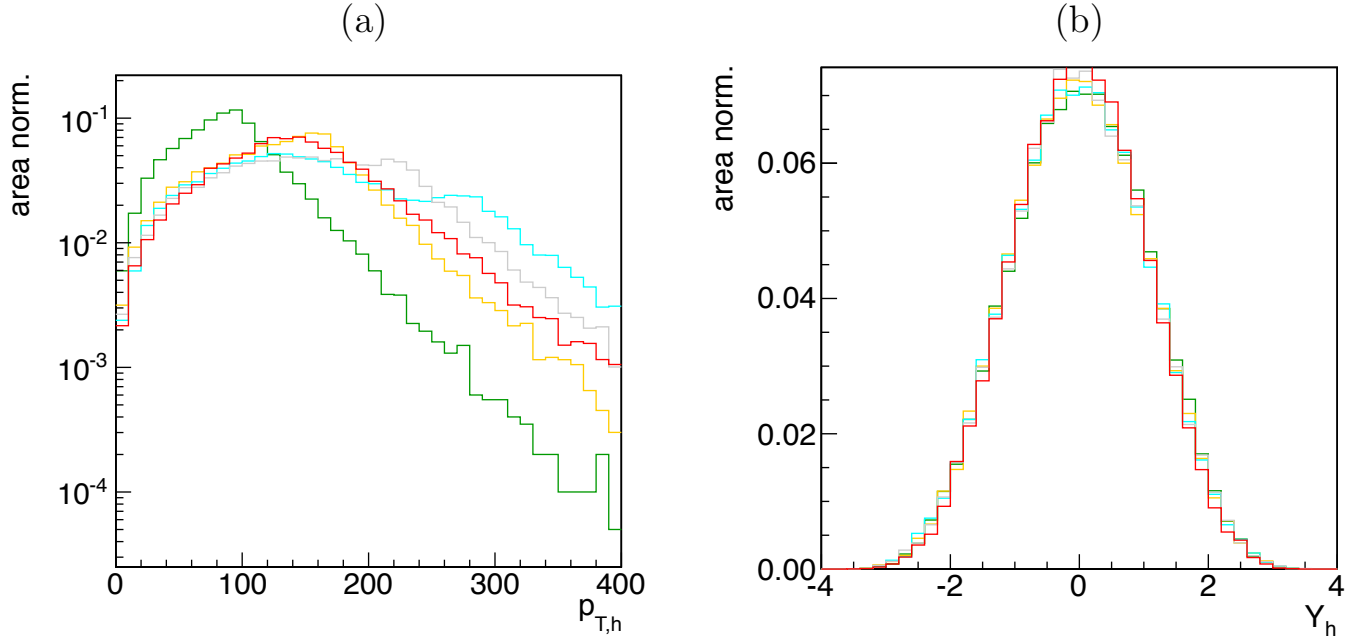


FIG. 5. Kinematic distributions for the  $p_{T,h}$  of the Higgs boson in di-Higgs production at LHC. Panel (a) shows  $(1/\sigma)d\sigma(gg \rightarrow hh)/dp_{T,h}$  for the SM alone (red) and the SM combined with loops of scalars,  $M_S = 160$  GeV (green),  $M_S = 200$  GeV (orange),  $M_S = 250$  GeV (gray) and  $M_S = 300$  GeV (cyan). The Higgs-portal has been taken to be  $\kappa = -1$  for all cases. The right panel shows the Higgs rapidity distribution  $(1/\sigma)d\sigma(gg \rightarrow hh)/dY_h$  for the same scalar values.

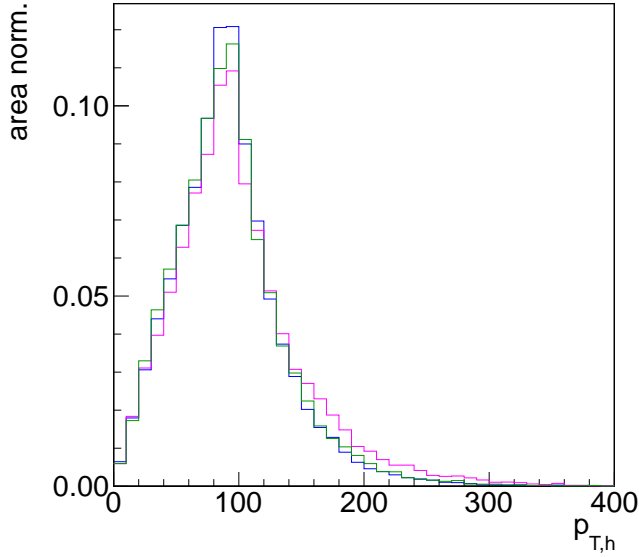


FIG. 6. Comparison between the  $p_{T,h}$  spectra in  $gg \rightarrow hh$  for three different values of  $\kappa$ . The scalar mass is held fixed at 160 GeV but we vary the Higgs-portal coupling;  $\kappa = -1.0$  (green),  $\kappa = -1.5$  (blue),  $\kappa = -0.5$  (magenta). The distributions are area normalized to focus on the shape differences.

for single Higgs production is constrained to be roughly the Standard Model value. As we saw from Sec. V A, given a range in the single Higgs production rate, there

is a corresponding range of  $\kappa, M_S$  parameter space. The wider the range, the larger the variation in the di-Higgs production rate.

Here we are interested in the absolute rate of di-Higgs production. While we have not calculated beyond one-loop, Ref. [3] found the  $K$  factor for di-Higgs production in the Standard Model to be  $\mathcal{O}(2)$ . This means  $\sigma(pp \rightarrow hh)/\sigma(pp \rightarrow h) \simeq 2500$  at  $\sqrt{s} = 8$  TeV. Because there are two Higgs bosons in the final state, the rate for di-Higgs to feed into any characteristic single-Higgs final state ( $\gamma\gamma + X, ZZ^* + X$ , etc.) is obviously doubled. We expect that these di-Higgs events would be captured by the inclusive single Higgs searches at the LHC. In the absence of an observation, this should allow ATLAS and CMS to obtain an estimate of the upper bound on the di-Higgs enhancement. Dedicated analyses of existing  $\sqrt{s} = 7$  and 8 TeV data that focus on the exact di-Higgs final state and kinematics, such as  $\gamma\gamma + \bar{b}b$ , would undoubtedly increase the sensitivity to the signal.

The discovery prospects for some di-Higgs final states, including with enhanced production rate, have been outlined in Ref. [20–22, 25, 26, 35]. However, in the time since those studies there have been significant advances in the usage of jet substructure as a discovery tool, for both hadronic ( $b\bar{b}$ ) [54–56] and  $\tau^+\tau^-$  [57, 58] resonances. Given the relatively high  $p_T$  that the Higgs bosons can carry, i.e., Fig. 5, we expect di-Higgs events to be well suited to substructure techniques.

The rates, in fb, for several potential di-Higgs final states are shown in Table I. All rates are functions of the

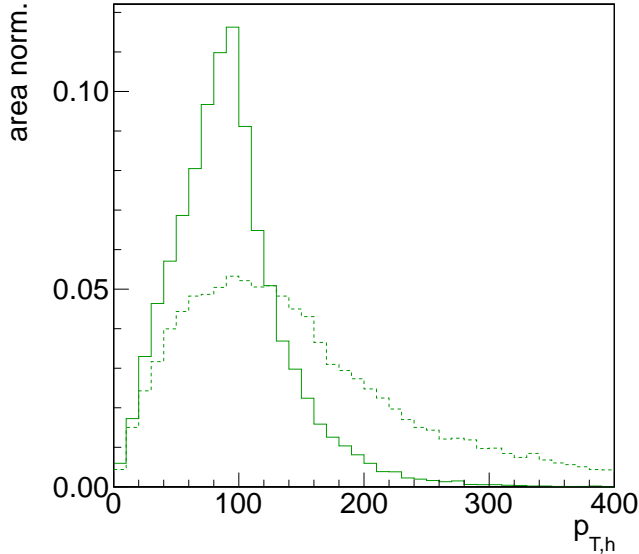


FIG. 7. The difference in the  $p_{T,h}$  spectrum of the Higgs bosons from di-Higgs production between using the full one-loop momentum dependence (solid line) versus the effective operators (dashed line). In this figure we have taken  $M_S = 150$  GeV,  $\kappa = -1$ . The distributions are area normalized to focus on the shape differences.

|                 | final state                | rates in fb |           |
|-----------------|----------------------------|-------------|-----------|
|                 |                            | 8 TeV       | 14 TeV    |
| $m_h = 125$ GeV | $\gamma\gamma + b\bar{b}$  | $0.019 X$   | $0.084 X$ |
|                 | $\tau^+\tau^- + b\bar{b}$  | $0.53 X$    | $2.4 X$   |
|                 | $\tau^+\tau^-\tau^+\tau^-$ | $0.029 X$   | $0.13 X$  |
| $m_h = 200$ GeV | $W^+W^-W^+W^-$             | $1.21 X$    | $5.73 X$  |
|                 | $ZZZZ$                     | $0.14 X$    | $0.68 X$  |
|                 | $W^+W^-ZZ$                 | $0.42 X$    | $1.97 X$  |

TABLE I. The di-Higgs signal production rates into the different modes when  $m_h = 125$  GeV and  $m_h = 200$  GeV. All rates, which include a K factor of 2.0, must be multiplied by the enhancement factor  $X$  which can be read off from the di-Higgs contours in Fig. 3 ( $m_h = 125$  GeV) and Fig. 4 ( $m_h = 200$  GeV).

enhancement  $X$  and we have taken the  $K$ -factor to be 2.0 throughout. We find that varying the parton distribution set changes the cross-section by  $\mathcal{O}(20\%)$ .

Now, in the alternative case  $m_h = 200$  GeV, the single Higgs production cross section is constrained to be less than the present LHC bounds. This basically requires us to choose  $(\kappa, M_S)$  within the red or blue region of Fig. 4. By taking  $m_h = 200$  GeV, both diboson decay modes are open, i.e.,  $m_h > 2m_W, 2m_Z$ , and the di-Higgs production phenomenology becomes fairly insensitive to the exact value of the Higgs mass. In Table I we show the rates for the various combinations of dibosons. The  $hh \rightarrow W^+W^-W^+W^-$  is the largest, and provides several opportunities involving same-sign dileptons or tripletons

plus missing energy. Here again, jet substructure techniques could provide valuable additional sensitivity given the large  $p_T$  of the Higgs bosons in di-Higgs production.

## VII. DISCUSSION

We have demonstrated that di-Higgs production at the LHC could be many orders of magnitude larger than the Standard Model in the presence of light colored scalars. The large enhancements are possible if  $m_h = 125$  GeV, consistent with the recent data from LHC, as well as if  $m_h > 125$  GeV, should the 125 GeV particle turn out to be a Higgs imposter. The latter region is natural in a model with light colored scalars, since this model was already demonstrated to effectively hide the Higgs below the LHC limits [12]. The largest effects occur when the Higgs-portal coupling  $\kappa$  is negative and colored scalars that are lighter than the electroweak breaking scale. Our detailed numerical results were performed in a model with a single, real, color octet scalar. Direct production of the colored scalar and decay to pairs of gluons is presently constrained by LHC data only for  $M_S \lesssim 125$  GeV. Hence, a wide range of  $(\kappa, M_S)$  space remains viable that can lead to the huge di-Higgs enhancement rates that we find.

Our calculation of the production rates were performed for a general set of colored scalars at leading order, and thus up to the overall multiplicity, are independent of the electroweak quantum numbers. The detailed branching fractions of the Higgs will, of course, depend on the electroweak quantum numbers. Generally this leads to  $\mathcal{O}(1)$  effects on the branching fractions, whereas the di-Higgs production rate enhancements we found can be orders of magnitude larger. It would be interesting to perform a more detailed investigation of the correlation between single Higgs production and decay, with other representations of colored scalars, versus the di-Higgs production cross section [11, 13, 59, 60]. In addition, electroweak charged scalars will alter a wider set of processes than electroweak singlets:  $pp \rightarrow VV$ , where  $V = \gamma, Z^0, W^\pm$  will all change due to loops of electroweak charged scalars, in addition to  $pp \rightarrow hh$ . Restricting to electroweak neutral colored scalars, we were somewhat forced to use octets. This is because smaller representations, for instance the color triplet or sextet, are *stable* when the scalars are electroweak singlets.

The signals of di-Higgs production provide several exciting opportunities for the LHC. We have already seen that di-Higgs production could have *already* contributed a fraction of the single Higgs production rate, with the second Higgs missed (or unidentified) in the events. If  $m_h = 125$  GeV, among the more interesting di-Higgs signals includes  $hh \rightarrow \gamma\gamma b\bar{b}$ ,  $hh \rightarrow \tau^+\tau^- b\bar{b}$ , and  $hh \rightarrow \tau^+\tau^-\tau^+\tau^-$ . Each of these signals has two pairs of particles that reconstruct to two Higgs bosons. If  $m_h > 125$  GeV, there are several channels resulting from  $hh \rightarrow W^+W^-W^+W^-$ , including same-sign leptons

plus missing energy as well as trileptons plus missing energy that could be seen at LHC. The latter two searches might first obtain evidence from recasted supersymmetric searches, while a more dedicated search strategy would undoubtedly improve the sensitivity. Jet substructure may also provide a valuable additional strategy for both low and high Higgs masses.

## Appendix A: Passarino-Veltman One-Loop Functions

The Passarino-Veltman functions are defined by:

$$C_0(p_i, p_j : m) = \int \frac{d^4 q}{i\pi} \frac{1}{(q^2 - m^2)((q + p_i)^2 - m^2)((q + p_i + p_j)^2 - m^2)} \quad (A1)$$

$$D_0(p_i, p_j, p_k : m) = \int \frac{d^4 q}{i\pi} \frac{1}{(q^2 - m^2)((q + p_i)^2 - m^2)((q + p_i + p_j)^2 - m^2)((q + p_i + p_j + p_k)^2 - m^2)} \quad (A2)$$

## Appendix B: Effective Couplings versus One-loop Results

Comparison of exact one-loop result against that obtained from using the effective couplings in Fig. 8. Here we only show a “zoomed in” region for small  $M_S$  and negative  $\kappa$ , where the differences between the calculations are largest. Nevertheless, we have verified that for  $M_i \gg v, m_h$ , the contours asymptotically agree.

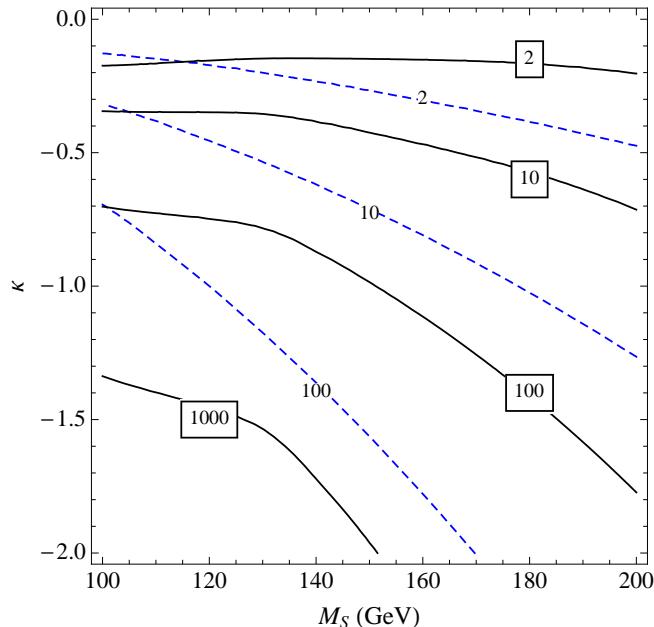


FIG. 8. Comparison of exact one-loop result against that obtained from using the effective couplings

## Appendix C: Renormalization Group Equations

The renormalization group equations for  $\kappa$ ,  $\omega$ , and  $\lambda_h$  (taking  $\mu_S$  to be small and negligible) are:

$$16\pi^2 \frac{d\kappa}{dt} = 2\kappa^2 - 9\kappa g_c^2 + 6\kappa\lambda_h + 10\kappa\omega \quad (C1)$$

$$16\pi^2 \frac{d\omega}{dt} = \kappa^2 + 24\omega^2 - 18g_c^2\omega + 12g_c^4 \quad (C2)$$

where  $g_c$  is the  $SU(3)$  coupling and  $\lambda_h$  is the Standard Model Higgs quartic coupling. All terms in the  $\kappa$  renormalization group equation are proportional to  $\kappa$ , since  $\kappa = 0$  is technically natural. The running of  $\lambda_h$  is also changed by the Higgs portal interaction:

$$16\pi^2 \frac{d\lambda_h}{dt} = \beta_{\lambda_h} + 4\kappa^2, \quad (C3)$$

where  $\beta_{\lambda_h}$  is the  $\beta$ -function for the Higgs quartic coupling coming from SM interactions.

For large positive  $\kappa$ , Eq. (C1) shows that  $\kappa$  will grow and ultimately hit a Landau pole, similar to what happens with the Higgs quartic coupling. For large negative  $\kappa$ , however, Eq. (C1) shows that the Higgs-portal interaction rapidly *decreases* until the other terms in the renormalization group equation become important. Hence, a one-loop renormalization group improved potential is necessary to analyze the stability of the effective potential in the presence of a large negative  $\kappa$  coupling. Our estimates suggest  $\kappa \gtrsim -2$  is perfectly acceptable, however a detailed analysis of the scalar potential is beyond the scope of this paper.

## ACKNOWLEDGMENTS

We thank B. Dobrescu for collaboration during the early part of this work, and Y. Gershtein for valuable conversations. GDK thanks the Theoretical Physics Group at Fermilab for warm hospitality where part of this work was completed. GDK was supported in part by the US

Department of Energy under contract number DE-FG02-96ER40969 as well as a URA Visiting Scholar Award from Fermilab. AM was supported by Fermilab oper-

ated by Fermi Research Alliance, LLC under contract number DE-AC02-07CH11359 with the US Department of Energy.

- 
- [1] E. W. N. Glover, J. J. van der Bij, Nucl. Phys. **B309**, 282 (1988).
  - [2] T. Plehn, M. Spira and P. M. Zerwas, Nucl. Phys. B **479**, 46 (1996) [Erratum-ibid. B **531**, 655 (1998)] [hep-ph/9603205].
  - [3] S. Dawson, S. Dittmaier and M. Spira, Phys. Rev. D **58**, 115012 (1998) [hep-ph/9805244].
  - [4] A. Djouadi, W. Kilian, M. Muhlleitner and P. M. Zerwas, Eur. Phys. J. C **10**, 45 (1999) [hep-ph/9904287].
  - [5] G. L. Kane, G. D. Kribs, S. P. Martin and J. D. Wells, Phys. Rev. D **53**, 213 (1996) [hep-ph/9508265]; S. Dawson, A. Djouadi and M. Spira, Phys. Rev. Lett. **77**, 16 (1996) [hep-ph/9603423]. A. Djouadi, Phys. Lett. B **435**, 101 (1998) [hep-ph/9806315]; M. S. Carena, S. Heinemeyer, C. E. M. Wagner and G. Weiglein, Eur. Phys. J. C **26**, 601 (2003) [hep-ph/0202167]; M. Muhlleitner and M. Spira, Nucl. Phys. B **790**, 1 (2008) [hep-ph/0612254]; I. Low and S. Shalgar, JHEP **0904**, 091 (2009) [arXiv:0901.0266]; A. Menon and D. E. Morrissey, Phys. Rev. D **79**, 115020 (2009) [arXiv:0903.3038];
  - [6] A. V. Manohar, M. B. Wise, Phys. Rev. D **74**, 035009 (2006) [hep-ph/0606172]; X. -G. He, G. Valencia, [arXiv:1108.0222].
  - [7] C. Arnesen, I. Z. Rothstein and J. Zupan, Phys. Rev. Lett. **103**, 151801 (2009) [arXiv:0809.1429].
  - [8] E. Ma, Phys. Lett. B **706**, 350 (2012) [arXiv:1109.4177]; [arXiv:1112.1367].
  - [9] R. Bonciani, G. Degrassi and A. Vicini, JHEP **0711**, 095 (2007) [arXiv:0709.4227]. U. Aglietti, R. Bonciani, G. Degrassi and A. Vicini, JHEP **0701**, 021 (2007) [hep-ph/0611266]; C. Anastasiou, *et al*, JHEP **0701**, 082 (2007) [hep-ph/0611236].
  - [10] R. Boughezal, F. Petriello, Phys. Rev. D **81**, 114033 (2010) [arXiv:1003.2046]; R. Boughezal, Phys. Rev. D **83**, 093003 (2011) [arXiv:1101.3769].
  - [11] Y. Bai, J. Fan and J. L. Hewett, arXiv:1112.1964 [hep-ph].
  - [12] B. A. Dobrescu, G. D. Kribs and A. Martin, arXiv:1112.2208 [hep-ph].
  - [13] B. Batell, S. Gori and L. -T. Wang, JHEP **1206**, 172 (2012) [arXiv:1112.5180 [hep-ph]].
  - [14] V. D. Barger and T. Han, Mod. Phys. Lett. A **5**, 667 (1990).
  - [15] K. Hagiwara and H. Murayama, Phys. Rev. D **41**, 1001 (1990).
  - [16] V. D. Barger, A. L. Stange and R. J. N. Phillips, Phys. Rev. D **45**, 1484 (1992).
  - [17] A. Djouadi, W. Kilian, M. Muhlleitner and P. M. Zerwas, Eur. Phys. J. C **10**, 27 (1999) [hep-ph/9903229].
  - [18] A. Belyaev, M. Drees, O. J. P. Eboli, J. K. Mizukoshi and S. F. Novaes, Phys. Rev. D **60**, 075008 (1999) [hep-ph/9905266].
  - [19] A. A. Barrientos Bendezu and B. A. Kniehl, Phys. Rev. D **64**, 035006 (2001) [hep-ph/0103018].
  - [20] U. Baur, T. Plehn and D. L. Rainwater, Phys. Rev. Lett. **89**, 151801 (2002) [hep-ph/0206024].
  - [21] U. Baur, T. Plehn and D. L. Rainwater, Phys. Rev. D **67**, 033003 (2003) [hep-ph/0211224].
  - [22] U. Baur, T. Plehn and D. L. Rainwater, Phys. Rev. D **69**, 053004 (2004) [hep-ph/0310056].
  - [23] M. Moretti, S. Moretti, F. Piccinini, R. Pittau and A. D. Polosa, JHEP **0502**, 024 (2005) [hep-ph/0410334].
  - [24] T. Plehn and M. Rauch, Phys. Rev. D **72**, 053008 (2005) [hep-ph/0507321].
  - [25] T. Binoth, S. Karg, N. Kauer and R. Ruckl, Phys. Rev. D **74**, 113008 (2006) [hep-ph/0608057].
  - [26] A. Pierce, J. Thaler, L. -T. Wang, JHEP **0705**, 070 (2007) [hep-ph/0609049].
  - [27] S. Dawson, C. Kao, Y. Wang and P. Williams, Phys. Rev. D **75**, 013007 (2007) [hep-ph/0610284].
  - [28] M. Moretti, S. Moretti, F. Piccinini, R. Pittau and J. Rathsmann, JHEP **0712**, 075 (2007) [arXiv:0706.4117 [hep-ph]].
  - [29] S. Kanemura, K. Tsumura, Eur. Phys. J. C **63**, 11-21 (2009) [arXiv:0810.0433].
  - [30] R. Lafaye, T. Plehn, M. Rauch, D. Zerwas and M. Duhrssen, JHEP **0908**, 009 (2009) [arXiv:0904.3866 [hep-ph]].
  - [31] A. Arhrib, R. Benbrik, C. -H. Chen, R. Guedes and R. Santos, JHEP **0908**, 035 (2009) [arXiv:0906.0387 [hep-ph]].
  - [32] M. Moretti, S. Moretti, F. Piccinini, R. Pittau and J. Rathsmann, JHEP **1011**, 097 (2010) [arXiv:1008.0820 [hep-ph]].
  - [33] E. Asakawa, D. Harada, S. Kanemura, Y. Okada and K. Tsumura, Phys. Rev. D **82**, 115002 (2010) [arXiv:1009.4670 [hep-ph]].
  - [34] R. Grober and M. Muhlleitner, JHEP **1106**, 020 (2011) [arXiv:1012.1562 [hep-ph]].
  - [35] R. Contino, M. Ghezzi, M. Moretti, G. Panico, F. Piccinini and A. Wulzer, arXiv:1205.5444 [hep-ph].
  - [36] M. J. Dolan, C. Englert and M. Spannowsky, arXiv:1206.5001 [hep-ph].
  - [37] G. Aad *et al.* [ATLAS Collaboration], [arXiv:1110.2693].
  - [38] CMS Collaboration, CMS PAS EXO-11-016
  - [39] G. Aad *et al.* [ATLAS Collaboration], arXiv:1207.0319 [hep-ex].
  - [40] CMS Collaboration, CMS-PAS-HIG-12-020.
  - [41] W. D. Goldberger and M. B. Wise, Phys. Lett. B **475**, 275 (2000) [arXiv:hep-ph/9911457], G. F. Giudice, R. Rattazzi and J. D. Wells, Nucl. Phys. B **595**, 250 (2001) [arXiv:hep-ph/0002178], C. Csaki, M. L. Graesser and G. D. Kribs, Phys. Rev. D **63**, 065002 (2001) [arXiv:hep-th/0008151], W. D. Goldberger, B. Grinstein and W. Skiba, Phys. Rev. Lett. **100** (2008) 111802 [arXiv:0708.1463 [hep-ph]], A. De Rujula, J. Lykken, M. Pierini, C. Rogan and M. Spiropulu, Phys. Rev. D **82**, 013003 (2010) [arXiv:1001.5300 [hep-ph]], I. Low and J. Lykken, JHEP **1010**, 053 (2010) [arXiv:1005.0872 [hep-ph]], H. Davoudiasl, T. McElmurry and A. Soni, Phys. Rev. D **82**, 115028 (2010) [arXiv:1009.0764 [hep-ph]], P. J. Fox, D. Tucker-Smith and N. Weiner, JHEP

- 1106**, 127 (2011) [arXiv:1104.5450 [hep-ph]].
- [42] J. R. Ellis, M. K. Gaillard and D. V. Nanopoulos, Nucl. Phys. B **106**, 292 (1976).
  - [43] M. A. Shifman, A. I. Vainshtein, M. B. Voloshin and V. I. Zakharov, Sov. J. Nucl. Phys. **30**, 711 (1979) [Yad. Fiz. **30**, 1368 (1979)].
  - [44] B. A. Kniehl and M. Spira, Z. Phys. C **69**, 77 (1995) [hep-ph/9505225].
  - [45] I. Low, R. Rattazzi and A. Vichi, JHEP **1004**, 126 (2010) [arXiv:0907.5413 [hep-ph]].
  - [46] M. Gillioz, R. Grober, C. Grojean, M. Muhlleitner and E. Salvioni, arXiv:1206.7120 [hep-ph].
  - [47] Y. Bai, B. A. Dobrescu, JHEP **1107**, 100 (2011). [arXiv:1012.5814].
  - [48] R. S. Chivukula, M. Golden, E. H. Simmons, Nucl. Phys. B **363** (1991) 83.
  - [49] B. A. Dobrescu, K. Kong, R. Mahbubani, Phys. Lett. B **670**, 119-123 (2008) [arXiv:0709.2378]; J. M. Arnold and B. Fornal, arXiv:1112.0003.
  - [50] J. Alwall, P. Demin, S. de Visscher, R. Frederix, M. Herquet, F. Maltoni, T. Plehn and D. L. Rainwater *et al.*, JHEP **0709**, 028 (2007) [arXiv:0706.2334 [hep-ph]].
  - [51] K. Hagiwara, H. Murayama and I. Watanabe, Nucl. Phys. B **367**, 257 (1991).
  - [52] H. Murayama, I. Watanabe and K. Hagiwara, KEK-91-11.
  - [53] T. Hahn and M. Perez-Victoria, “Automatized one loop calculations in four-dimensions and D-dimensions,” Comput. Phys. Commun. **118**, 153 (1999) [hep-ph/9807565].
  - [54] J. M. Butterworth, A. R. Davison, M. Rubin and G. P. Salam, Phys. Rev. Lett. **100**, 242001 (2008) [arXiv:0802.2470 [hep-ph]].
  - [55] A. Abdesselam, E. B. Kuutmann, U. Bitenc, G. Brooijmans, J. Butterworth, P. Bruckman de Renstrom, D. Buarque Franzosi and R. Buckingham *et al.*, Eur. Phys. J. C **71**, 1661 (2011) [arXiv:1012.5412 [hep-ph]].
  - [56] A. Altheimer, S. Arora, L. Asquith, G. Brooijmans, J. Butterworth, M. Campanelli, B. Chapleau and A. E. Cholakian *et al.*, J. Phys. G **39**, 063001 (2012) [arXiv:1201.0008 [hep-ph]].
  - [57] A. Katz, M. Son and B. Tweedie, Phys. Rev. D **83**, 114033 (2011) [arXiv:1011.4523 [hep-ph]].
  - [58] C. Englert, T. S. Roy and M. Spannowsky, Phys. Rev. D **84** (2011) 075026 [arXiv:1106.4545 [hep-ph]].
  - [59] S. Mantry, M. Trott and M. B. Wise, Phys. Rev. D **77**, 013006 (2008) [arXiv:0709.1505 [hep-ph]].
  - [60] J. M. Arnold, M. Pospelov, M. Trott and M. B. Wise, JHEP **1001**, 073 (2010) [arXiv:0911.2225 [hep-ph]].